Solution-Processable Singlet Fission Photovoltaic Devices

*Le Yang[1], Maxim Tabachnyk[1], Sam L. Bayliss[1], Marcus L. Böhm[1], Katharina Broch[1], Neil C. Greenham[1], Richard H. Friend[1], Bruno Ehrler[1,2]**

[1] Cavendish Laboratory, J J Thomson Avenue, Cambridge CB3 0HE, United Kingdom

[2] FOM Institute AMOLF, Science Park 104, 1098 XG Amsterdam, The Netherlands

ABSTRACT

We demonstrate the successful incorporation of a solution-processable singlet fission material, 6,13-bis(triisopropylsilylethynyl)pentacene (TIPS-pentacene), into photovoltaic devices. TIPS-pentacene rapidly converts high-energy singlet excitons into pairs of triplet excitons via singlet fission, potentially doubling the photocurrent from high-energy photons. Low-energy photons are captured by small-bandgap electron-accepting lead chalcogenide nanocrystals. This is the first solution-processable singlet fission system that performs with substantial efficiency, with maximum power conversion efficiencies exceeding 4.8%, and external quantum efficiencies of up to 60% in the TIPS-pentacene absorption range. With PbSe nanocrystal of suitable bandgap, its internal quantum efficiency reaches 170±30%.

KEYWORDS Singlet Fission, TIPS-Pentacene, Colloidal Nanocrystals, Hybrid Photovoltaics, Multiple Carrier Generation, Quantum Dots.

Singlet fission is an exciton multiplication mechanism in organic molecules, converting one singlet exciton into a pair of triplet excitons. It can occur on an ultrafast timescale (pico- or even femto-second) when the triplet state has approximately half the singlet energy, out-competing singlet decay via fluorescence.[1,2] Singlet fission has recently attracted considerable attention because it provides a path to overcome the single-junction Shockley-Queisser limit in solar cells by reducing thermalization losses.[2,3] To benefit from singlet fission, a large-bandgap singlet fission material has to be coupled to a small-bandgap semiconductor that acts as an electron acceptor and generates a single exciton per absorbed low-energy photon.[4,5]

Pentacene has been the first singlet fission material to be successfully implemented in working solar cells, with external quantum efficiencies (EQE) of up to 126% in pentacene/C_{60} solar cells when light trapping was employed, with internal quantum efficiencies (IQE) approaching 200%.[5–7] Bilayer cells with pentacene and infrared-absorbing inorganic nanocrystals as electron acceptors have been demonstrated with PbS and PbSe. The power conversion efficiency (PCE) of the PbS cells reached nearly 1%;[8] and with PbSe, the PCE improved to 4.7%.[9,10] The EQE obtained in these devices peaked at 80%, though the EQE at pentacene absorption peak (670 nm) was 30%.[9]

Despite these encouraging results, the instability in air and light hinders the commercial prospects of solar cells made from pentacene. Pentacene undergoes photo-oxidation, forming an endoperoxide as oxygen bridges across the C6 and C13 positions which are most susceptible to oxidation.[11–13]

Pentacene is insoluble in most common solvents so it needs to be deposited by thermal evaporation under vacuum. 6,13-bis(triisopropylsilylethynyl)pentacene (TIPS-pentacene) was

originally designed for good charge mobility in field-effect transistors,[14–17] and it shows a dramatically enhanced solubility and oxidative stability in solution.[18,19] Besides protecting the susceptible C6 and C13 positions with the bulky TIPS groups,[20] it has been suggested by Fudickar and Linker that they also help to ensure cycloreversion of the endoperoxide to the parent acene, preventing its further decomposition.[13] Maliakal et al. demonstrated theoretically that the TIPS groups lower the triplet energy of the acene, preventing singlet oxygen formation; and that they also lower the LUMO energy, minimizing charge transfer.[11,12] However, empirically both its triplet energy and LUMO were not found to be lower than unsubstituted pentacene.[21]

In concentrated solutions, TIPS-pentacene shows a triplet yield of 200%, with singlet fission occurring via a transient excimer intermediate, formed when one photoexcited molecule collides with a ground-state molecule.[21] In thin films of TIPS-pentacene, singlet fission is found to occur on a timescale of 1 ps with a triplet yield of 144%.[22] However, solar cells based on TIPS-pentacene have so far delivered limited promise. Lloyd et al. achieved a PCE of 0.52% with solution-processed TIPS-pentacene/C_{60} bilayer devices.[23] A separate study on vacuum sublimed TIPS-pentacene/C_{60} devices showed a PCE of 0.42%.[24]

Meanwhile, colloidal nanocrystals have garnered widespread interest in solar cells of various designs,[25–29] recently reaching a PCE of 8.55%.[30] By careful control of reaction temperature and time, nanocrystal size can be easily tuned, which inversely correlates to the bandgap energy. Monodispersity is crucial for good performance, to give an optimal compact arrangement of the nanocrystals and a clean energy landscape.[31] Small-bandgap nanocrystals absorb well into the red and near-infrared region, capturing low energy photons and making them ideal electron acceptors for low-energy TIPS-pentacene triplet excitons.

Here we report the incorporation of solution-processed TIPS-pentacene into photovoltaic devices with small-bandgap PbS or PbSe nanocrystals as the acceptor material, obtaining a PCE of 4.8% and an EQE of up to 60% in the region where TIPS-pentacene absorbs. We find that the IQE exceeds 100% for the TIPS-pentacene layer, unless the energetics of the nanocrystals do not allow for triplet exciton dissociation, in which case the IQE nearly halves.

The nanocrystal/TIPS-pentacene bilayer device architecture is shown in **Figure 1**. Electrons are transported through TiO_2 and extracted from ITO, while holes are extracted through the gold top contact (**Figure 1c**). Contrary to previous pentacene/nanocrystal bilayer architectures,[8–10] TIPS-pentacene needs to be deposited on top of the cross-linked nanocrystals layer due to a lack of orthogonal solvents. We find that the thicknesses of individual neat films add up to that of the bilayer film. Furthermore the absorption peak of the PbS nanocrystals remains unchanged when TIPS-pentacene is spun on top (**Supporting Information Figure S4**). This suggests that the two components do not react with each other, in contrast to TIPS-pentacene and fullerenes.[32,33]

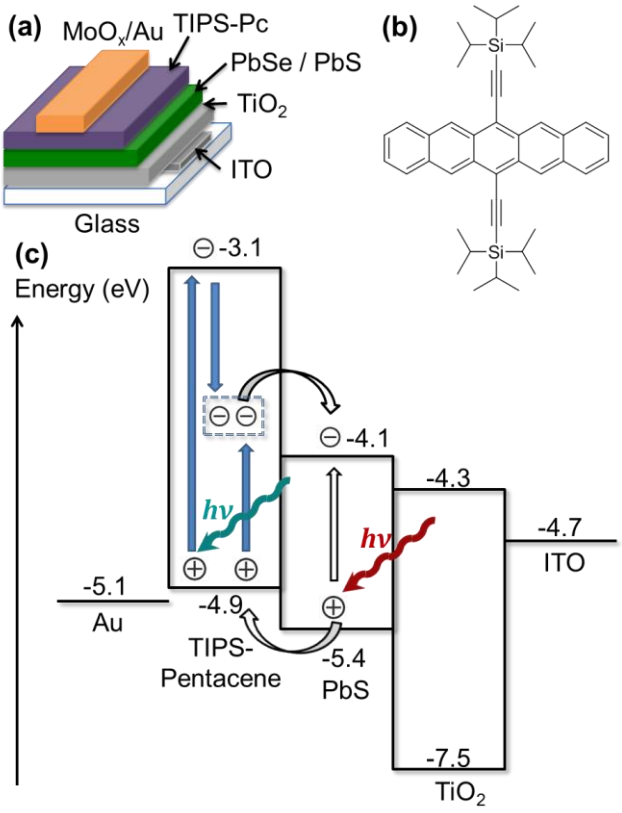

Figure 1 (a) Device architecture of the nanocrystal/TIPS-pentacene photovoltaic device. **(b)** Chemical structure of TIPS-pentacene. **(c)** Alignment of energy levels in the PbS/TIPS-pentacene device. Blue arrows illustrate the singlet fission process in TIPS-pentacene upon photoexcitation. When PbSe is used instead of PbS, this energy diagram remains similar except for the valence band of PbSe being at -5.1 eV, and its conduction band varies accordingly. TIPS-pentacene HOMO and nanocrystal valence bands were determined by ultraviolet photoelectron spectroscopy (UPS) as described by Ehrler et al.[9]

An inherent shortcoming of this device structure is that light is incident from the bottom of the substrate, passing through the nanocrystal layer first where up to 85% of the light is absorbed. This diminishes the EQE contribution from TIPS-pentacene. Using a transparent top and reflective bottom contact can potentially circumvent this limitation (see detailed discussion in the **Supporting**

Information Section 3), as TIPS-pentacene receives a larger fraction of light as it is incident from the top.

Surface ligands on the nanocrystals are crucial for charge transport and interfacial properties with acenes.[34,35] The long, insulating native ligands (oleic acid) on the nanocrystals are exchanged for shorter, more conductive ligands in a solid-state process.[36] Common ligands such as tetrabutylammonium iodide (TBAI), 1,2-ethanedithiol (EDT), and benzene-1,3-dithiol (BDT) have been used as shorter ligands for improved charge transport.[30] Even though the heterojunction between TIPS-pentacene and all the aforementioned combinations led to devices with considerable performance and charge generation from both materials (**Supporting Information Section 4**), subsequent experiments and optimization were done with BDT capped PbSe and PbS for consistency and ease of fabrication.

Figure 2 shows the power conversion efficiency (PCE) and open-circuit voltage (V_{oc}) of nanocrystal/TIPS-pentacene devices for a range of nanocrystal sizes (PbSe in **Figure 2a** and PbS in **Figure 2b**). All parameters are enhanced with larger bandgap for each series. The increase in open-circuit voltage (V_{oc}) with increasing nanocrystal bandgap in both series corresponds to the increase in diagonal bandgap between the donor-acceptor layers. Together with the higher fill factor measured (see **Table S2 and S3 in the Supporting Information**), this raises the PCE of the device. Under various optimized conditions, V_{oc} as high as 0.60 V and short-circuit current (J_{sc}) up to 21.4 mA/cm^2 have been achieved, with a champion cell producing a PCE of 4.8% (**Figure 2c,** and see **Section 5 of Supporting Information** for full solar cell characterization).

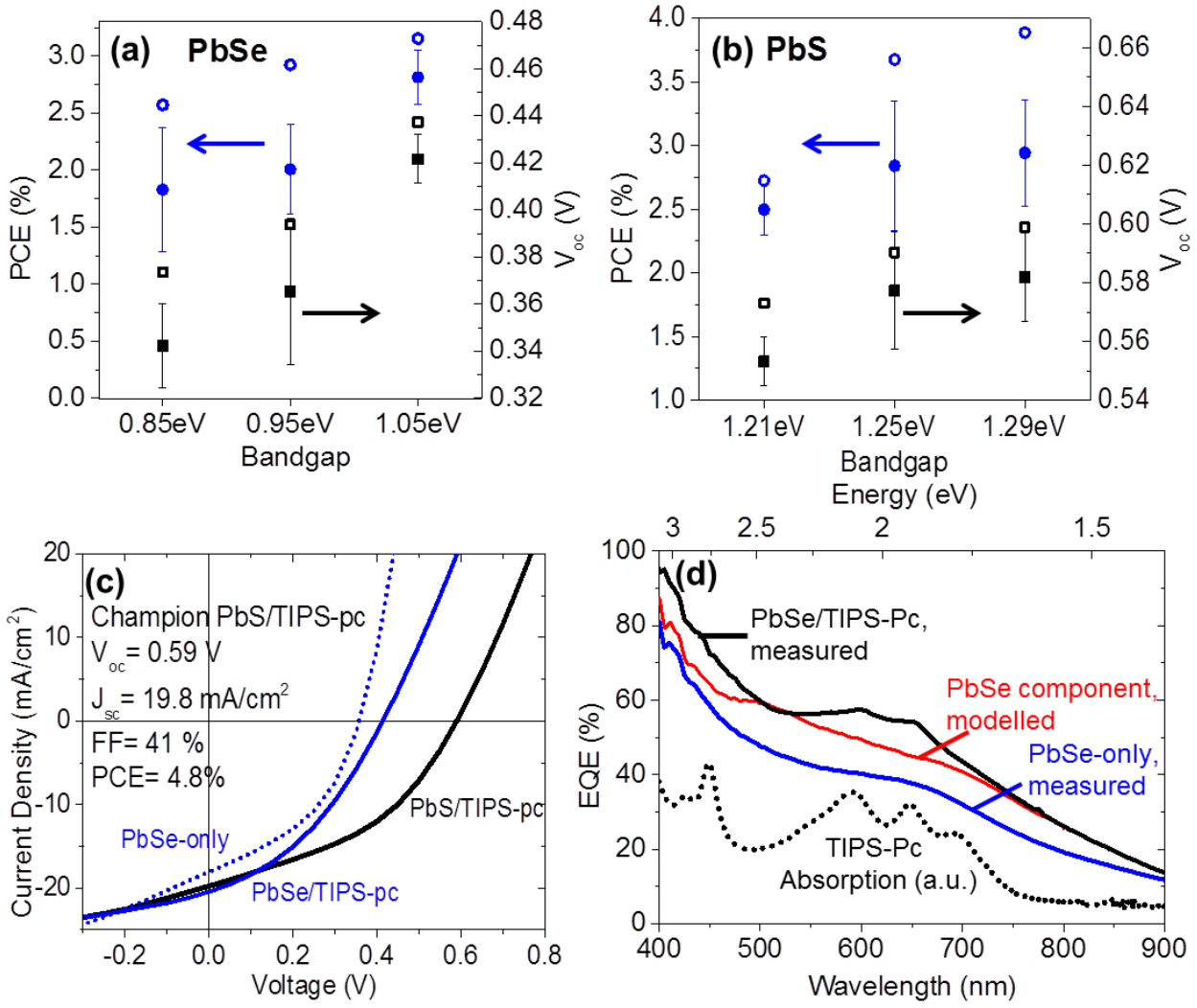

Figure 2 Device PCE and V_{oc} variation with bandgap of **(a)** PbSe and **(b)** PbS in the nanocrystal/TIPS-pentacene devices, all fabricated under similar conditions. Unfilled data points represent the best performance under these conditions. **(c)** The I-V characteristics of the 1.25 eV PbS/TIPS-pentacene champion cell (upon further optimization, specifically of the duration of BDT soaking time, see **Supporting Information Section 1.3** for details), with PCE exceeding 4.8% in comparison to a device made from TIPS-pentacene and PbSe and a device made from PbSe only. **(d)** EQE spectrum of a PbSe/TIPS-pentacene device compared to that of a PbSe-only device of the same bandgap.

Figure 2d shows a typical EQE spectrum of a PbSe-only device in comparison with a PbSe/TIPS-pentacene device. The underlying shape of the PbSe/TIPS-pentacene spectrum follows that of the PbSe-only spectrum, as the majority of light is being absorbed and converted into photocurrent by the PbSe (70-85% in the range 500-700 nm). The peaks seen at 591 nm and 648 nm follow the features of the absorption of a TIPS-pentacene film, indicating that there is significant photocurrent contribution from TIPS-pentacene over the spectral region from ~550-700 nm. It is noteworthy that the EQE over this region reaches up to 60%. Interestingly, we only see photocurrent generation from the TIPS-pentacene features at 648 nm and 591 nm, but not at 692 nm. This peak at 692 nm has been assigned to an aggregate feature of TIPS-pentacene film due to improved packing of the molecules.[21,37] In photoluminescence (PL) measurements on thick neat TIPS-pentacene films, its emission peak occurs at 667 nm (**Supporting Information Figure S3**). The absence of an emission from the lowest-energy 692 nm peak, whose absorption is associated with aggregates,[21,37] indicates that these states efficiently recombine non-radiatively, explaining their absence EQE spectra of all the devices.

The presence of a positive EQE contribution from TIPS-pentacene in all the devices suggests that the conduction band edges of all the PbSe/PbS used in our study are low enough to ionize the triplets generated from singlet fission in TIPS-pentacene, leading to net electron transfer from TIPS-pentacene to the nanocrystals. Analogous to previous studies on PbSe/pentacene bilayer devices,[9] we expect a negative contribution towards the overall EQE from TIPS-pentacene when the bandgap of the nanocrystal is sufficiently large such that the conduction band level is too high to ionize the triplets (**Figure 3a**). Thus when TIPS-pentacene is combined with 1.3 eV bandgap PbSe, this EQE contribution is reduced, with the remaining contribution presumably from the low-

bandgap tail of the nanocrystal distribution and possibly from some direct singlet exciton transfer prior to singlet fission (**Figure 3b**).

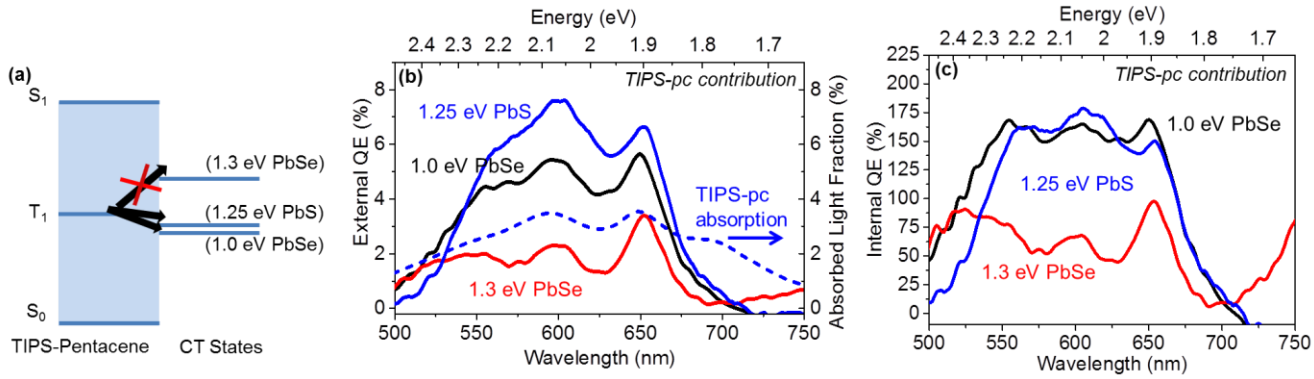

Figure 3 (a) Energy alignment between the TIPS-pentacene triplet state and the charge transfer (CT) states with different nanocrystals bandgaps (in brackets), where the CT energy is approximated by the difference between the nanocrystal conduction band energy and the TIPS-pentacene highest occupied molecular orbital (HOMO). **(b)** EQE contribution and modelled absorbed light fraction from TIPS-pentacene; and **(c)** IQE of TIPS-pentacene in bilayer devices with nanocrystals of different bandgaps, isolated from total EQE by transfer matrix optical modelling.

To investigate the origin of the TIPS-pentacene photocurrent, transfer matrix optical modelling was performed to calculate the absorption profile of the device which then allows the extraction of the internal quantum efficiency (IQE) (**Supporting Information Section 6**).[7,38] It is assumed that the heterojunction consists of a sharp and flat interface between the layers. We first modelled the PbSe-only IQE from the measured EQE of PbSe-only devices. This IQE can then be used to model the PbSe EQE component of the overall EQE in a PbSe/TIPS-pentacene device. The difference between the measured overall EQE of a PbSe/TIPS-pentacene device and this PbSe component

represents the TIPS-pentacene component of the EQE (**Figure 3b**), since PbSe and TIPS-pentacene are the only active layers contributing towards photocurrent. The IQE of TIPS-pentacene can be obtained by using its isolated EQE contribution divided by its absorbed light fraction (**Equation 1**). We observe an IQE above 100% in TIPS-pentacene only when the acceptor level in the nanocrystals is low enough for triplet ionization (**Figure 3c**). Since we deposit only a very thin layer of TIPS-pentacene (16±4 nm), any variation in the thickness-dependent light absorption will lead to a large change in the output IQE. To estimate this uncertainty, we determined the IQE for the range of model parameters that gave a good fit (**Supporting Information Section 6.1**). We found that with small-bandgap PbSe (1.0 eV), the TIPS-pentacene IQE in the ~550-700 nm range reaches up to 160±40%, while with 1.3 eV PbSe the TIPS-pentacene IQE drops to 80±20% (**Figure 3c**). This confirms that singlet fission is operational in the devices with small-bandgap nanocrystals. Despite accurate determination of the TIPS-pentacene contribution to the photocurrent from our optical modelling, we still observe no sign of photocurrent from the aggregate feature at 692 nm.

$$IQE_{TIPS-pc} = \frac{EQE_{overall,measured} - EQE_{PbSe,modelled}}{Absorption_{TIPS-pc}}$$ – **Equation 1**

Naively, one may expect that adding bulky, inactive TIPS groups to pentacene may prohibit charge/exciton transport. However, the high IQE we find provides clear evidence of effective photocurrent generation in these devices.

We recognize that the optical modelling is very sensitive to the TIPS-pentacene layer thickness. Jadhav et al. also pointed out that scattering and light trapping can lead to further uncertainty in estimating the absorption in polyacene films.[39] To provide corroborative evidence for singlet fission contributing to the photocurrent, we measured the effect of magnetic field on the photocurrent of the devices. As described by Merrifield,[40] an applied magnetic field changes the rate of triplets

fusing back to emissive singlets and shifts the equilibrium in the concentrations of singlet and triplet excitons. As already demonstrated for other acenes,[10,40] an increase in photoluminescence from pristine TIPS-pentacene can be seen when applying a magnetic field (**Figure 4**, blue trace), associated with an increased ratio of emissive singlets to dark triplets. In solar cells, we expect a reduction in photocurrent if the dominant photocurrent contribution from TIPS-pentacene is from triplets. Indeed, we observe a drop in photocurrent for devices made from a thin layer (~40-60 nm) of 0.95 eV bandgap PbSe and 1.25 eV PbS with TIPS-pentacene, while no change is observed for nanocrystal-only devices (Error! Reference source not found.). This drop indicates pronounced triplet contribution to the photocurrent for both devices. We note that the magnitude of photocurrent change is not indicative of the fraction of triplets contributing to the photocurrent, as the majority of the photocurrent is produced by the nanocrystals, which are slightly different in the two devices. For larger bandgap nanocrystals we observe no photocurrent change within the resolution of our experimental setup (<0.05%, see **Figure 4** and **Supporting Information Section 1.6** for additional bandgaps). This indicates that the photocurrent we observe from TIPS-pentacene in the large-bandgap PbSe devices could have originated from a mixture of singlet and triplet excitons extracted through the low-bandgap tail of the nanocrystal distribution. Lower-bandgap nanocrystals can extract the triplet excitons more efficiently, hence the higher IQE.

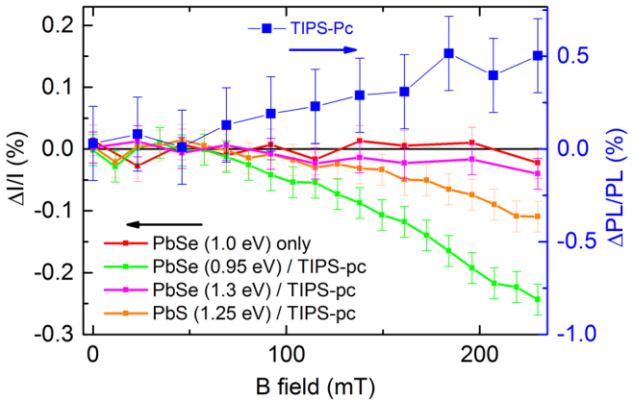

Figure 4 Magnetic field response of photoluminescence (PL) of a pristine TIPS-pentacene film and of photocurrent in nanocrystals/TIPS-pentacene devices. All samples were excited with a laser at 637 nm.

In conclusion we have demonstrated a single-junction two-bandgap solar cell with all active layers processed from solution. In a bilayer heterojunction architecture with lead chalcogenide nanocrystals, these TIPS-pentacene devices show promising efficiencies of more than 4.8%, achieving a maximum V_{oc} of more than 0.6 V with PbS nanocrystals and J_{sc} of more than 20 mA/cm^2 with PbSe nanocrystals. The internal quantum efficiency exceeds 100% in devices with nanocrystal bandgaps that allow for triplet ionization.

ASSOCIATED CONTENT

Supporting Information. A summary of experimental methods, UV-Vis absorption spectra, supporting figures on the optical modelling of IQE, additional figures and data of device I-V characteristics can be found in the Supporting Information. This material is available free of charge via the Internet at http://pubs.acs.org.

AUTHOR INFORMATION

Corresponding Author

*Email: b.ehrler@amolf.nl

Author Contributions

The manuscript was written through contributions of all authors. All authors have given approval to the final version of the manuscript.

Notes

The authors declare no competing financial interests.

ACKNOWLEDGMENT

L.Y. thanks Dr Dawei Di, Guangru Li, Tom Jellicoe and Dr Brian Walker for useful discussion and experimental advice; Nathaniel Davis for large bandgap PbSe; and the Singapore Agency of Science, Technology and Research (A*STAR) for financial assistance. M.T. thanks that the Gates Cambridge Trust, the Winton Programme for Sustainability and the EPSRC for funding. S.L.B. also thanks the EPSRC for funding. M.L.B thanks the German National Academic Foundation (Studienstiftung) for funding. K.B. thanks the German Research Foundation for funding (BR 4869/1-1). B.E. thanks Selwyn College Cambridge and KACST for funding.

REFERENCES

(1) Smith, M. B.; Michl, J. *Annu. Rev. Phys. Chem.* **2013**, *64*, 361–386.

(2) Smith, M. B.; Michl, J. *Chem. Rev.* **2010**, *110*, 6891–6936.

(3) Shockley, W.; Queisser, H. J. *J. Appl. Phys.* **1961**, *32*, 510–519.

(4) Lee, J.; Jadhav, P.; Reusswig, P. D.; Yost, S. R.; Thompson, N. J.; Congreve, D. N.; Hontz, E.; Van Voorhis, T.; Baldo, M. A. *Acc. Chem. Res.* **2013**, *46*, 1300–1311.

(5) Congreve, D. N.; Lee, J.; Thompson, N. J.; Hontz, E.; Yost, S. R.; Reusswig, P. D.; Bahlke, M. E.; Reineke, S.; Van Voorhis, T.; Baldo, M. A. *Science* **2013**, *340*, 334–337.

(6) Thompson, N. J.; Congreve, D. N.; Goldberg, D.; Menon, V. M.; Baldo, M. A. *Appl. Phys. Lett.* **2013**, *103*, 263302.

(7) Tabachnyk, M.; Ehrler, B.; Bayliss, S.; Friend, R. H.; Greenham, N. C. *Appl. Phys. Lett.* **2013**, *103*, 153302.

(8) Ehrler, B.; Wilson, M. W. B.; Rao, A.; Friend, R. H.; Greenham, N. C. *Nano Lett.* **2012**, *12*, 1053–1057.

(9) Ehrler, B.; Walker, B. J.; Böhm, M. L.; Wilson, M. W. B.; Vaynzof, Y.; Friend, R. H.; Greenham, N. C. *Nat. Commun.* **2012**, *3*, 1019.

(10) Jadhav, P. J.; Brown, P. R.; Thompson, N.; Wunsch, B.; Mohanty, A.; Yost, S. R.; Hontz, E.; Van Voorhis, T.; Bawendi, M. G.; Bulović, V.; Baldo, M. A. *Adv. Mater.* **2012**, *24*, 6169–6174.

(11) Maliakal, A.; Raghavachari, K.; Katz, H.; Chandross, E.; Siegrist, T. *Chem. Mater.* **2004**, *16*, 4980–4986.

(12) Northrop, B. H.; Houk, K. N.; Maliakal, A. *Photochem. Photobiol. Sci.* **2008**, *7*, 1463–1468.

(13) Fudickar, W.; Linker, T. *J. Am. Chem. Soc.* **2012**, *134*, 15071–15082.

(14) Lee, S. H.; Choi, M. H.; Han, S. H.; Choo, D. J.; Jang, J.; Kwon, S. K. *Org. Electron.* **2008**, *9*, 721–726.

(15) Anthony, J. E.; Brooks, J. S.; Eaton, D. L.; Parkin, S. R. *J. Am. Chem. Soc.* **2001**, *123*, 9482–9483.

(16) Park, S. K.; Jackson, T. N.; Anthony, J. E.; Mourey, D. a. *Appl. Phys. Lett.* **2007**, *91*, 063514.

(17) Giri, G.; Verploegen, E.; Mannsfeld, S. C. B.; Atahan-Evrenk, S.; Kim, D. H.; Lee, S. Y.; Becerril, H. a; Aspuru-Guzik, A.; Toney, M. F.; Bao, Z. *Nature* **2011**, *480*, 504–508.

(18) Anthony, J. E.; Eaton, D. L.; Parkin, S. R. *Org. Lett.* **2002**, *4*, 15–18.

(19) Park, S. K.; Mourey, D. a.; Han, J.-I.; Anthony, J. E.; Jackson, T. N. *Org. Electron.* **2009**, *10*, 486–490.

(20) Li, Y.; Wu, Y.; Liu, P.; Prostran, Z.; Gardner, S.; Ong, B. S. *Chem. Mater.* **2007**, *19*, 418–423.

(21) Walker, B. J.; Musser, A. J.; Beljonne, D.; Friend, R. H. *Nat. Chem.* **2013**, *5*, 1019–1024.

(22) Ramanan, C.; Smeigh, A. L.; Anthony, J. E.; Marks, T. J.; Wasielewski, M. R. *J. Am. Chem. Soc.* **2012**, *134*, 386–397.

(23) Lloyd, M. T.; Mayer, A. C.; Tayi, A. S.; Bowen, A. M.; Kasen, T. G.; Herman, D. J.; Mourey, D. A.; Anthony, J. E.; Malliaras, G. G. *Org. Electron.* **2006**, *7*, 243–248.

(24) Palilis, L. C.; Lane, P. A.; Kushto, G. P.; Purushothaman, B.; Anthony, J. E.; Kafafi, Z. H. *Org. Electron.* **2008**, *9*, 747–752.

(25) Semonin, O. E.; Luther, J. M.; Choi, S.; Chen, H.-Y.; Gao, J.; Nozik, A. J.; Beard, M. C. *Science* **2011**, *334*, 1530–1533.

(26) Ko, D.-K.; Brown, P. R.; Bawendi, M. G.; Bulović, V. *Adv. Mater.* **2014**, *26*, 4845–4850.

(27) Tisdale, W. A.; Williams, K. J.; Timp, B. A.; Norris, D. J.; Aydil, E. S.; Zhu, X.-Y. *Science* **2010**, *328*, 1543–1547.

(28) Nozik, A. J.; Beard, M. C.; Luther, J. M.; Law, M.; Ellingson, R. J.; Johnson, J. C. *Chem. Rev.* **2010**, *110*, 6873–6890.

(29) Kramer, I. J.; Sargent, E. H. *Chem. Rev.* **2014**, *114*, 863–882.

(30) Chuang, C. M.; Brown, P. R.; Bulović, V.; Bawendi, M. G. *Nat. Mater.* **2014**, 1–6.

(31) Zhitomirsky, D.; Kramer, I. J.; Labelle, A. J.; Fischer, A.; Debnath, R.; Pan, J.; Bakr, O. M.; Sargent, E. H. *Nano Lett.* **2012**, *12*, 1007–1012.

(32) Briggs, J. B.; Miller, G. P. *Comptes Rendus Chim.* **2006**, *9*, 916–927.

(33) Lloyd, M. T.; Anthony, J. E.; Malliaras, G. G. *Mater. Today* **2007**, *10*, 34–41.

(34) Ip, A. H.; Thon, S. M.; Hoogland, S.; Voznyy, O.; Zhitomirsky, D.; Debnath, R.; Levina, L.; Rollny, L. R.; Carey, G. H.; Fischer, A.; Kemp, K. W.; Kramer, I. J.; Ning, Z.; Labelle, A. J.; Chou, K. W.; Amassian, A.; Sargent, E. H. *Nat. Nanotechnol.* **2012**, *7*, 577–582.

(35) Tabachnyk, M.; Ehrler, B.; Gélinas, S.; Böhm, M. L.; Walker, B. J.; Musselman, K. P.; Greenham, N. C.; Friend, R. H.; Rao, A. *Nat. Mater.* **2014**, *13*, 1033–1038.

(36) Konstantatos, G.; Clifford, J.; Levina, L.; Sargent, E. H. *Nat. Photonics* **2007**, *1*, 531–534.

(37) Hwang, D. K.; Fuentes-Hernandez, C.; Berrigan, J. D.; Fang, Y.; Kim, J.; Potscavage, W. J.; Cheun, H.; Sandhage, K. H.; Kippelen, B. *J. Mater. Chem.* **2012**, *22*, 5531–5537.

(38) Burkhard, G. F.; Hoke, E. T.; McGehee, M. D. *Adv. Mater.* **2010**, *22*, 3293–3297.

(39) Jadhav, P. J.; Mohanty, A.; Sussman, J.; Lee, J.; Baldo, M. a. *Nano Lett.* **2011**, *11*, 1495–1498.

(40) Merrifield, R. E.; Avakian, P.; Groff, R. P. *Chem. Phys. Lett.* **1969**, *3*, 155–157.

TOC GRAPHICS

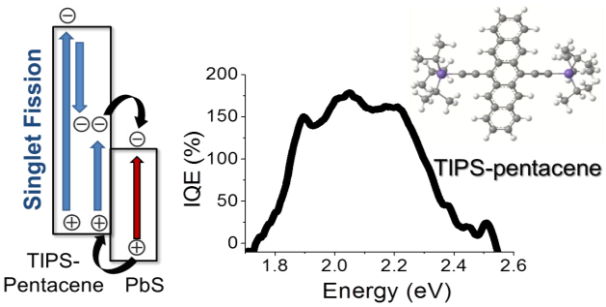
Singlet Fission
TIPS-
Pentacene
PbS
IQE (%)
200
150
100
50
0
1.8
2.0
2.2
2.4
2.6
Energy (eV)
TIPS-pentacene

Supporting Information

Solution-Processable Singlet Fission Photovoltaic Devices

Le Yang, Maxim Tabachnyk, Sam L. Bayliss, Marcus L. Böhm, Katharina Broch, Neil C. Greenham, Richard H. Friend, Bruno Ehrler

1. Experimental Methods

1.1 Materials

Lead(II) acetate (99.999%, $Pb(CH_3COO)_2.3H_2O$), oleic acid (technical grade, 90%, OA), 1-octadecene (technical grade, 90%, ODE), trioctylphosphine (97%, TOP), lead(II) oxide (99.999%, PbO), bis(trimethylsilyl)sulfide (synthesis grade, TMS), diphenhylphosphine (98%, DPP), toluene (99.8%, anhydrous), hexane (95%, anhydrous), ethanol (>99.5%, anhydrous), methanol (99.8%, anhydrous), 1-butanol (99.8%, anhydrous), chloroform (99%, anhydrous), acetonitrile (99.8%, anhydrous), benzene-1,3-dithiol (>99.0% BDT), tetrabutylammonium iodide (>99.0%, TBAI), 1,2-ethanedithiol (≥98.0%, EDT), and titanium(IV) isopropoxide (97%, TTIP) were purchased from Sigma-Aldrich. Selenium powder (99.999%, Se) was purchased from Alfa Aesar, and 6,13-Bis(triisopropylsilylethynyl)pentacene (TIPS-pentacene) was purchased from Ossila. All chemicals were used as received.

1.2 Nanocrystal Synthesis

PbSe and PbS nanocrystals were synthesized based on previously reported colloidal synthesis.[1–4]

PbSe Nanocrystals: Nanocrystal size (diameter and bandgap) can be carefully tuned by varying the reaction time and injection temperature. PbSe were synthesized with bandgap 0.85 – 1.30 eV. $Pb(OAc)_2.3H_2O$ (5.78 mmol, 2.20 mg) and OA (14.1 mmol, 4.45 mL) were dissolved in ODE (106 mmol, 34 mL). The reaction mixture was degassed under vacuum (10^{-2} mbar) at room temperature and subsequently at 100 °C. Coordination of oleate ligands to lead was completed at 170 °C in 1 h under nitrogen atmosphere. The selenide precursor was prepared by dissolving selenium (16.2 mmol, 1.28 g) and DPP (0.925 mmol, 161 µL) in TOP (36.3 mmol, 16.2 mL), and injected rapidly into the reaction mixture, held at 160 °C, under nitrogen. After 10 to 240 seconds of growth, the mixture was quenched by cold hexane and cooled to room temperature by an ice-cold water bath. Purification steps were performed under inert atmosphere via repeated cycles of dissolving in hexane, and precipitation with ethanol or 1-butanol/methanol mixture. Finally PbSe nanocrystals were re-dissolved in octane.

PbS Nanocrystals: PbS nanocrystals were synthesized in a bandgap range of 1.21 – 1.29 eV. PbO (2.0 mmol, 0.45 g) and OA (4.73 mmol, 1.5 mL) were dissolved in ODE (62.5 mmol, 20 mL) and

degassed under vacuum at 100°C. The sulfide precursor was prepared by dissolving TMS (1.0 mmol, 213 µL) and DPP (0.60 mmol, 104 µL) in degassed ODE (31.25 mmol, 10 mL). The precursor mixture was then injected rapidly into the reaction mixture at 120 – 170 °C under nitrogen. The heating mantle was removed and the flask was subsequently allowed to cool to 35 °C. Purification steps were the same as for PbSe except that toluene was used as the solvent. PbS nanocrystals were re-dispersed in octane for spin coating.

1.3 Device Fabrication

Indium tin oxide (ITO)-patterned substrates (Psiotec) were cleaned by sonication in acetone and IPA for 10 min each. The substrates were then subjected to oxygen plasma etching (250 W_f / 0 W_r, 10 min). The electron-transporting TiO_2 layer was deposited by atomic layer deposition (ALD), at 200-225 ^{0}C under vacuum, using $TiCl_4$ and water as precursors, cycled 500-1000 times, leading to a thickness of 25-50 nm. In some instances, the TiO_2 was prepared by sol-gel method.[5] Here, the titanium precursor was prepared by mixing solutions of TTIP (0.60 mmol, 175 µL) and 2 M hydrochloric acid (0.35 mmol, 17.5 µL) in ethanol (21.4 mmol, 1.25 mL each). The precursor mixture was filtered and spun on ITO substrates at 2000 rpm. These sol-gel TiO_2-covered substrates were annealed in air at 500 °C for 30 min. All TiO_2-covered substrates were subsequently taken into a nitrogen-filled glovebox for spin-coating of the active layer. Layer-by-layer deposition of PbSe and PbS was carried out following the original method described by Sargent et al.[6] A solution of the crosslinker BDT was prepared in acetonitrile (0.10-0.23% v/v). When other ligands were used, TBAI (1-10 mg/mL in MeOH) and EDT (0.02% v/v, in acetonitrile) would replace BDT. BDT was firstly spun on the TiO_2 layer, after a 5-10 s soak (30 s with the optimized batches), to create a crosslinking surface for PbSe or PbS nanocrystals. Excess BDT was then washed off with acetonitrile. Each layer was formed by spin-coating PbSe or PbS (25 mg/mL in octane), followed by crosslinking using BDT. Excess BDT was rinsed off by acetonitrile, and oleic ligands and unlinked nanocrystals were washed off by octane. All layers were filtered and spun at 1500 rpm for 10-15 s. For most devices, layers of PbSe or PbS of 90-130 nm were deposited. Solutions of TIPS-pentacene were prepared in chloroform (2 to 2.5 mg/mL) and spun through a filter on top of nanocrystals layers at 1500 rpm for 40-50 s (~13 - 20 nm). Top electrodes consisting of a thin layer of hole-transporting MoO_x (7-15 nm) and gold (80 nm) were deposited by thermal evaporation under vacuum at a pressure of 5×10^{-6} mbar. Finally, the devices were legged for electrical contact during measurements, and encapsulated with glass slides and transparent epoxy before being taken out into ambient atmosphere for characterization. External quantum efficiency (EQE) was measured with an Oriel Cornerstone 260 monochromator, within a wavelength range of 375-900 nm. Current-voltage characteristics were taken with an Oriel 92250A solar simulator and a Keithley 2636A source-measure unit.

1.4 Optical Properties & Film Thickness

UV-Vis absorption measurements of films, spun on glass Spectrosils, were performed with Hewlett Packard 8453 UV-Vis Spectrophotometer. The nanocrystals bandgap was determined by UV-Vis absorption (Perkin-Elmer Lambda 9 UV/VIS/NIR Spectrophotometer) of dilute solutions in tetrachloroethylene. Film thicknesses were measured with atomic force microscopy (AFM, Nanoscope IIIa). Thicknesses were subsequently checked with modelled thicknesses from ellipsometry data, and also in some cases with X-ray reflectivity (XRD).

1.5 Ellipsometry Measurements

TiO_2 and TIPS-pentacene were spincoated, and MoO_x evaporated, on silicon substrates, for which variable angle ellipsometry was performed in reflection, using a J. A. Woollam M-2000L Spectroscopic Ellipsometre with a 75W Xe light source and monochromator. TIPS-pentacene was also spincoated on glass substrates for additional variable angle ellipsometry measurements in transmission. The film thicknesses were fitted with a Cauchy model, with a starting value based on an estimate by AFM (and for TIPS-pentacene, based on an accurate determination by XRD due to its very thin thickness), over their transparent regions. TiO_2 and MoO_x were then fitted to a layered optical model using a point-by-point fit, and subsequently a normal fit, to result in a set of Kramers-Kronig consistent refractive indices (n) and extinction coefficients (k) for their entire wavelength range. For TIPS-pentacene, a multisample analysis was performed to extract its uniaxial anisotropic optical properties,[7] also using a point-by-point fit and subsequently a normal fit, to produce a set of Kramers-Kronig consistent n and k, over its entire wavelength range, parallel and perpendicular to the sample plane respectively. The specific models used for TIPS-pentacene on silicon and glass substrates are:

	Silicon	**Glass**
Layer 1	Si (substrate), 1 mm	Glass (substrate), 1 mm
Layer 2	SiO_x, 2 nm	n, k in-plane, 0 nm
Layer 3	n, k in-plane, 0 nm	n, k out-of-plane, 0 nm
Layer 4	n, k out-of-plane, 0 nm	Uniaxial layer, 16 nm
Layer 5	Uniaxial layer, 16 nm	

Nanocrystals (PbSe and PbS) were spincoated on silicon substrates as above and measured using a Woollam Vase VB-400 ellipsometer with monochromatic light using a Xe lamp and monochromator. Samples were measured in reflection and fitted with a model combining a Cauchy and two Gaussian components. All n and k extracted are shown in **Figure S1**.

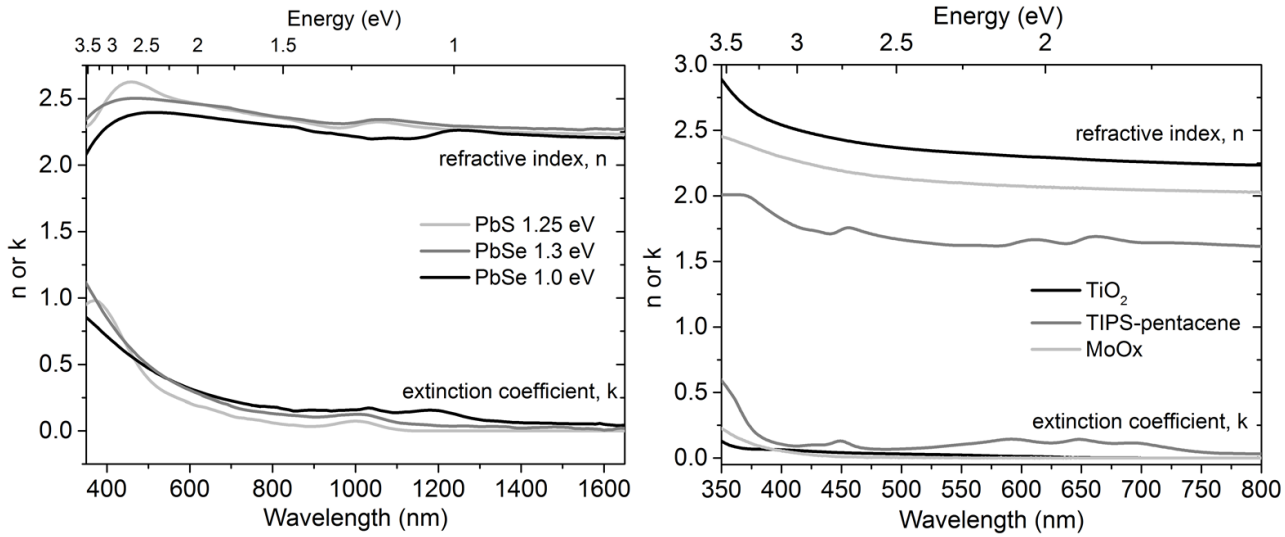

Figure S1 Modelled refractive indices (n) and extinction coefficients (k) of films obtained by ellipsometry.

1.6 Magneto-Photocurrent and -Photoluminescence Measurements

Photocurrent Response to Magnetic Field

The devices with much thinner nanocrystals layers (of 40-60 nm) were placed between the poles of an electromagnet (GMW Model 3470). A cw-diode laser (Thorlabs CPS635S) at 637 nm with an intensity below 5 mW/cm^2, chopped at 467 Hz, was used as the pump. The photocurrent was measured with a lock-in amplifier (Stanford SR830). For each magnetic field B, we averaged the B-field response over many cycles. In each cycle n, we

1. ramped up the B-field linearly from 0 T over 15 s
2. waited 10 s
3. measured the photocurrent with B-field ($I_{B,n}$) by averaging over 10 s with 0.5 s between each data point
4. ramped the B-field linearly down to 0 T for 15 s
5. waited 10 s
6. measured the photocurrent with no magnetic field ($I_{0,n}$) as above.

The photocurrent response was calculated by averaging $(I_{B,n} - ((I_{0,n-1}+I_{0,n})/2)) / ((I_{0,n-1}+I_{0,n})/2)$ over 20 cycles. We chose the excitation intensity low to avoid degradation artefacts and made sure that the baseline photocurrent decreases by less than 2% during the full measurement.

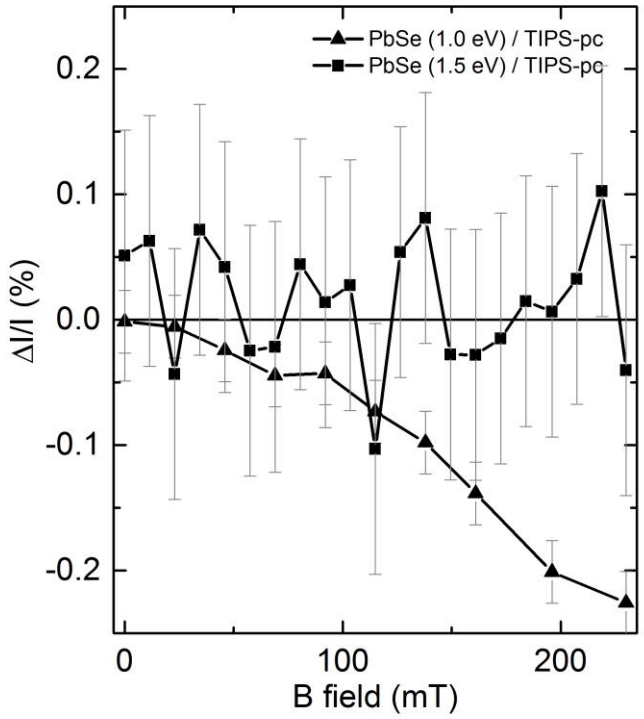

Figure S2. Magnetic field response for the photocurrent of nanocrystal/TIPS-pentacene devices and the photoluminescence of a neat TIPS-pentacene film. The noise for the 1.5 eV PbSe device is considerably higher because the overall photocurrent was lower.

Photoluminescence Response to Magnetic Field

The photoluminescence (PL) was measured by illuminating a spot of ca. 1 mm in diameter with a diode lasers (Thorlabs CPS635S) at 637 nm. Lenses project the PL emitted to a solid angle of 0.1 π onto an InGaAs detector (Andor DU490A-1.7). The sample was placed in an electromagnet (GMW Model 3470), and tilted around the vertical axis so that the pump was incident (and the PL was measured) at an angle of 60^0. A 650nm long-pass filter reflected scattered pump light before the PL entered the detector. The magneto-response was calculated with 3 cycles as for the photocurrent response, using the peak in the PL spectrum (**Figure S3**).

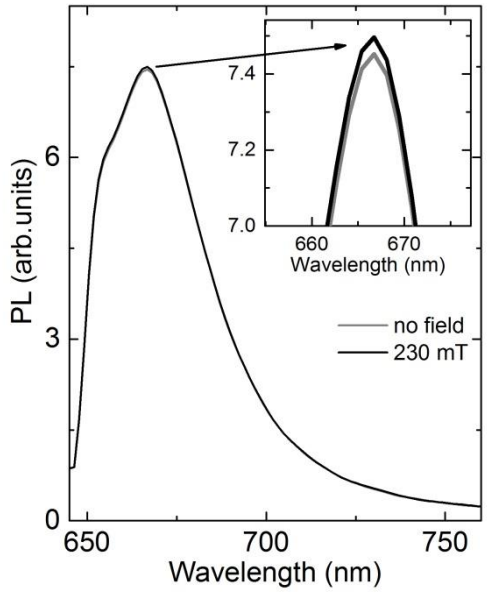

Figure S3. Extraction of the change in TIPS-pentacene PL under applied magnetic field.

2. UV-Vis Absorption Spectra

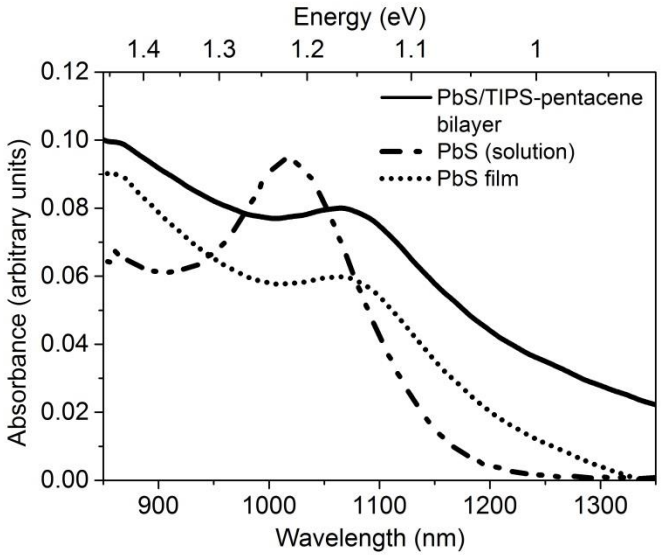

Figure S4 UV-Vis absorption of PbS film, PbS/TIPS-pentacene bilayer and PbS solution. There is a red shift of the peak from solution to film as observed before.[8] The 1.21 eV PbS (in solution) shifts to 1.16 eV in a neat film. This peak does not change in position when TIPS-pentacene is spun on top, but we do observe a higher degree of scattering.

3. Transparent Top Contact Devices: IQE Modelling

For a detailed description of the IQE modelling and associated error ranges, see **Section 6** of this document.

Using the IQEs calculated for TIPS-pentacene and PbSe, we demonstrate that a more pronounced EQE contribution would be obtained for a device with transparent top contacts (**Figure S5a**). All optical modelling for the 1.0 eV PbSe/TIPS-pentacene system has been done with the standard- device structure as shown in **Figure 1a** of the main text, with the active layer thicknesses as in **Table S4**. The EQE of such a device (black curve in **Figure S5b**) is then compared to the modelled EQE using the same parameters and IQEs but with a transparent top electrode (red curve in **Figure S5b**). Hence, the parameters modelled for the device with transparent top contact are (from the top of device): ITO (40 nm), TIPS-pentacene (16 nm), PbSe (95 nm), TiO_2 (85 nm), and Ag (50 nm). To date we have not been able to deposit transparent ITO contacts on top of TIPS pentacene. Alternatives such as thin metal electrodes may be a possibility towards this device configuration.[11]

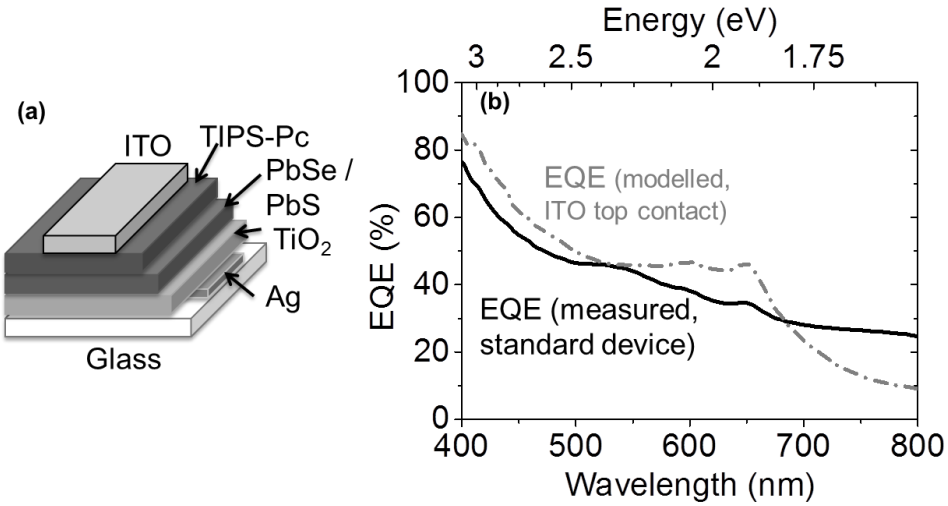

Figure S5 (a) Proposed device structure with a transparent top (ITO) and reflective bottom contact (Ag). **(b)** Modelled EQE of the proposed device structure (with 1.0 eV PbSe/TIPS-pentacene, and assuming the calculated IQE values) can result in a more pronounced photocurrent contribution from TIPS-pentacene.

4. Different PbS Surface Ligands: PbS/TIPS-pentacene Device I-V Data

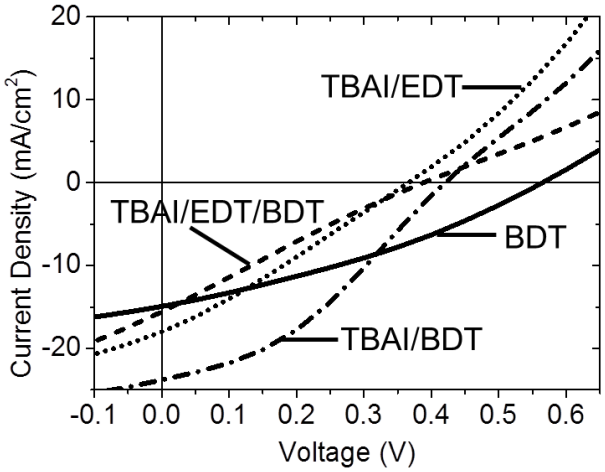

Figure S6 I-V curves of 1.21 eV PbS/TIPS-pentacene devices with different surface ligands, exchanged in solid-state during device fabrication. All devices were fabricated under similar conditions for fair comparison.

Table S1 I-V characteristics of devices shown in **Figure S2.**

	V_{oc} (V)	J_{sc} (mA/cm^2)	FF (%)	PCE (%)
BDT	0.565	14.93	32.33	2.72
TBAI / BDT	0.421	21.42	36.06	3.25
TBAI / EDT / BDT	0.389	20.04	23.46	1.83
TBAI / EDT	0.366	18.00	27.20	1.79

5. Additional Device Characteristics

The devices shown in this section were all fabricated under similar conditions, in particular similar duration of BDT soaking time (5-10 s). Longer soaking time of up to 30 s further optimized the devices, eventually producing the champion cell in Figure 2c in the main text.

Table S2 I-V characteristics of PbSe/TIPS-pentacene devices with increasing PbSe bandgap (which are able to ionize triplet excitons of TIPS-pentacene).

	V_{oc} (V)	J_{sc} (mA/cm^2)	FF (%)	PCE (%)
0.85eV PbSe / TIPS-Pentacene	0.281	14.58	27.32	1.12
0.95eV PbSe / TIPS-Pentacene	0.342	18.02	38.22	2.35
1.05eV PbSe / TIPS-Pentacene	0.413	20.43	37.31	3.15

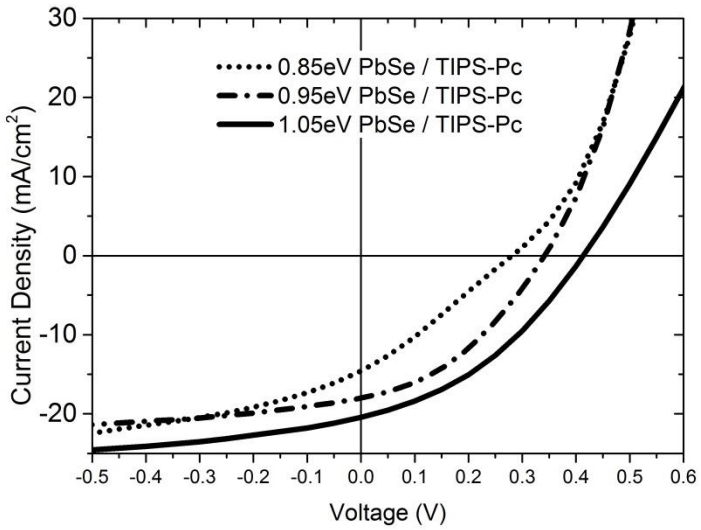

Figure S7 I-V curves of PbSe/TIPS-pentacene devices, with increasing PbSe bandgap (but able to ionize triplet excitons of TIPS-pentacene).

Table S3 I-V characteristics of PbS/TIPS-pentacene devices with increasing PbS bandgap small enough to ionize triplets from TIPS-pentacene.

	V_{oc} (V)	J_{sc} (mA/cm^2)	FF (%)	PCE (%)
1.21eV PbS / TIPS-Pentacene	0.554	12.27	39.40	2.68
1.25eV PbS / TIPS-Pentacene	0.559	16.02	41.07	3.68
1.29eV PbS / TIPS-Pentacene	0.581	15.65	42.76	3.89

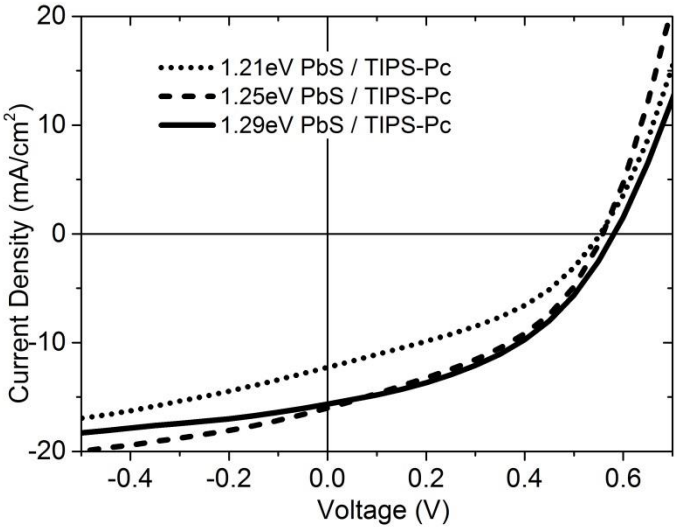

Figure S8 I-V characteristics of PbSe/TIPS-pentacene devices with increasing PbS bandgap small enough to ionize triplets from TIPS-pentacene.

6. Optical Modelling: IQE Calculations

The refractive indices (n) and extinction coefficients (k) of TiO_2, MoO_x, PbSe, PbS and TIPS-pentacene films were measured by ellipsometry, while those of Au[9] were taken from literature. The n and k values for ITO and Ag are taken from Burkhard, as well as the script for the transfer matrix method.[10]

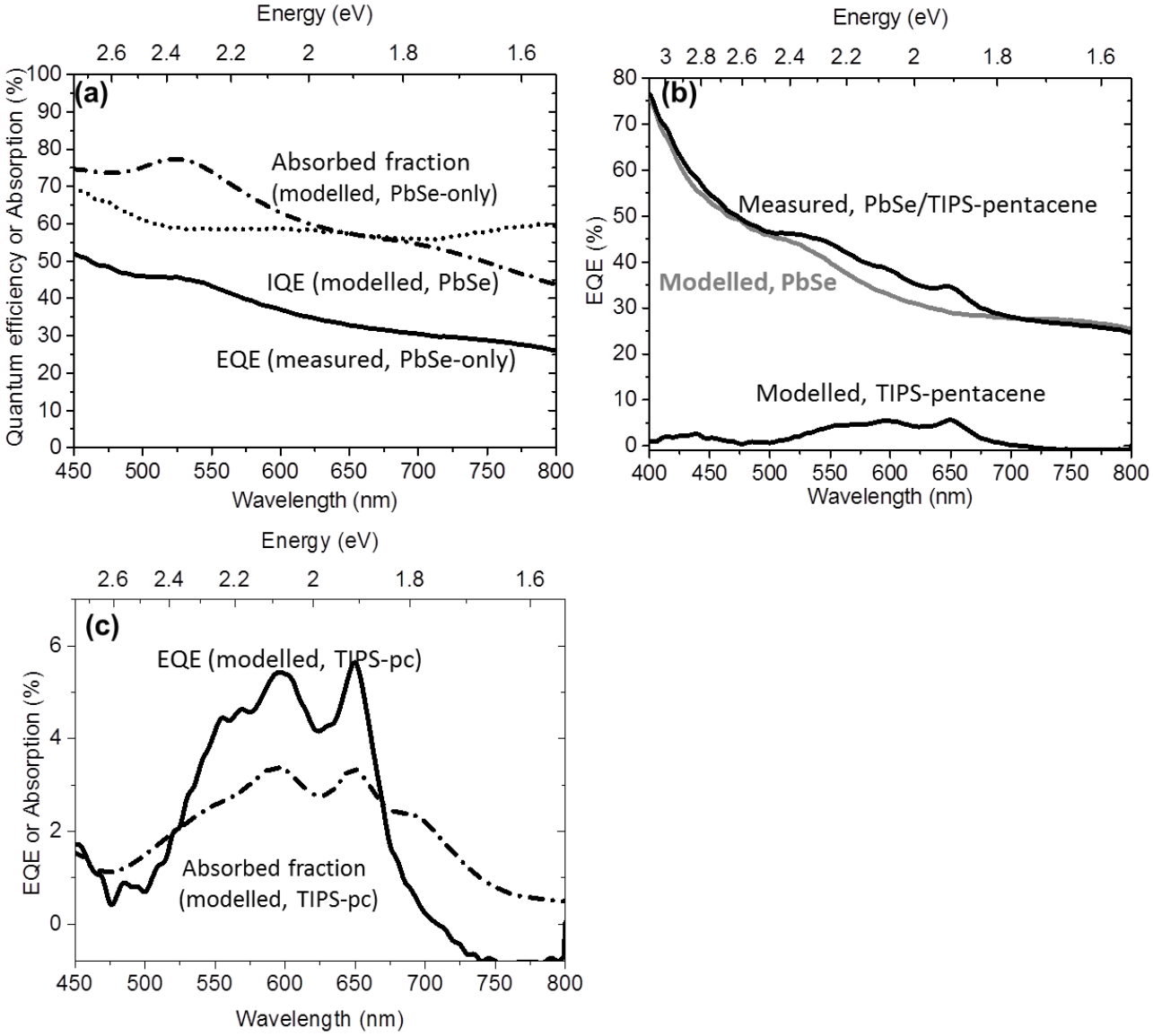

Figure S9 Transfer matrix optical modelling performed on 1.0 eV PbSe and 1.0 eV PbSe/TIPS-pentacene devices. In **(a)**, the EQE spectrum of a PbSe-only device was measured (black solid), and its absorbed light fraction (dash-dot) was obtained by the optical model. The IQE of the PbSe (dot) was then calculated by dividing the measured EQE (black solid) by its absorption (dash-dot). In **(b)**, using this PbSe IQE, we modelled the PbSe component (grey solid) of a PbSe/TIPS-pentacene device EQE. The TIPS-pentacene component (black solid, in (c)) of the device EQE was obtained by subtracting the PbSe component (grey solid) from the measured device EQE. The TIPS-pentacene IQE (**Figure 3c** of the main text) was finally obtained by dividing the TIPS-pentacene EQE (black solid in (c)) by its modelled absorbed light fraction (dash-dot, in (c)). For exact parameters used, refer to **Table S4**.

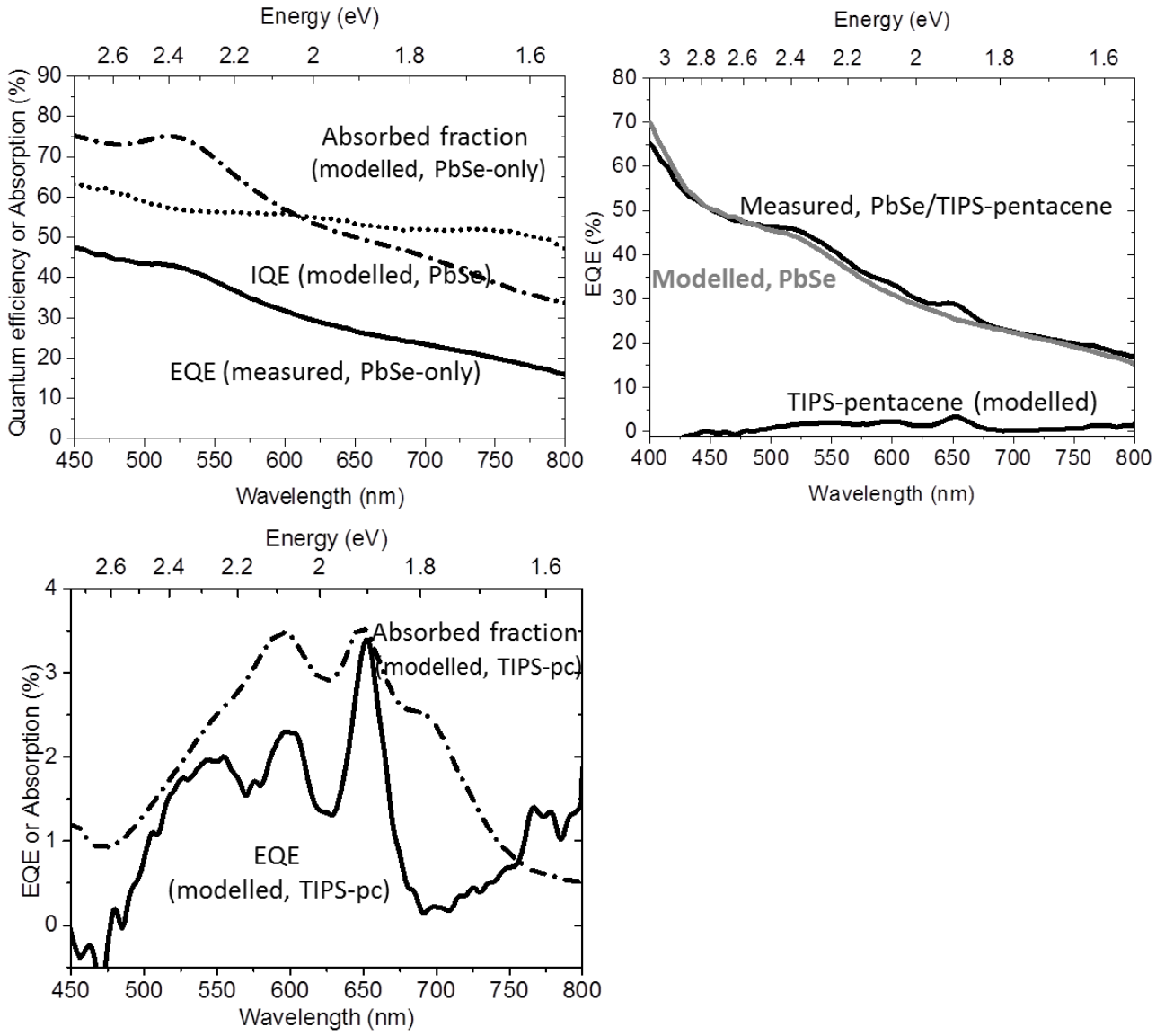

Figure S10 As above (**Figure S5**), for the 1.3 eV PbSe and 1.3 eV PbSe/TIPS-pentacene devices.

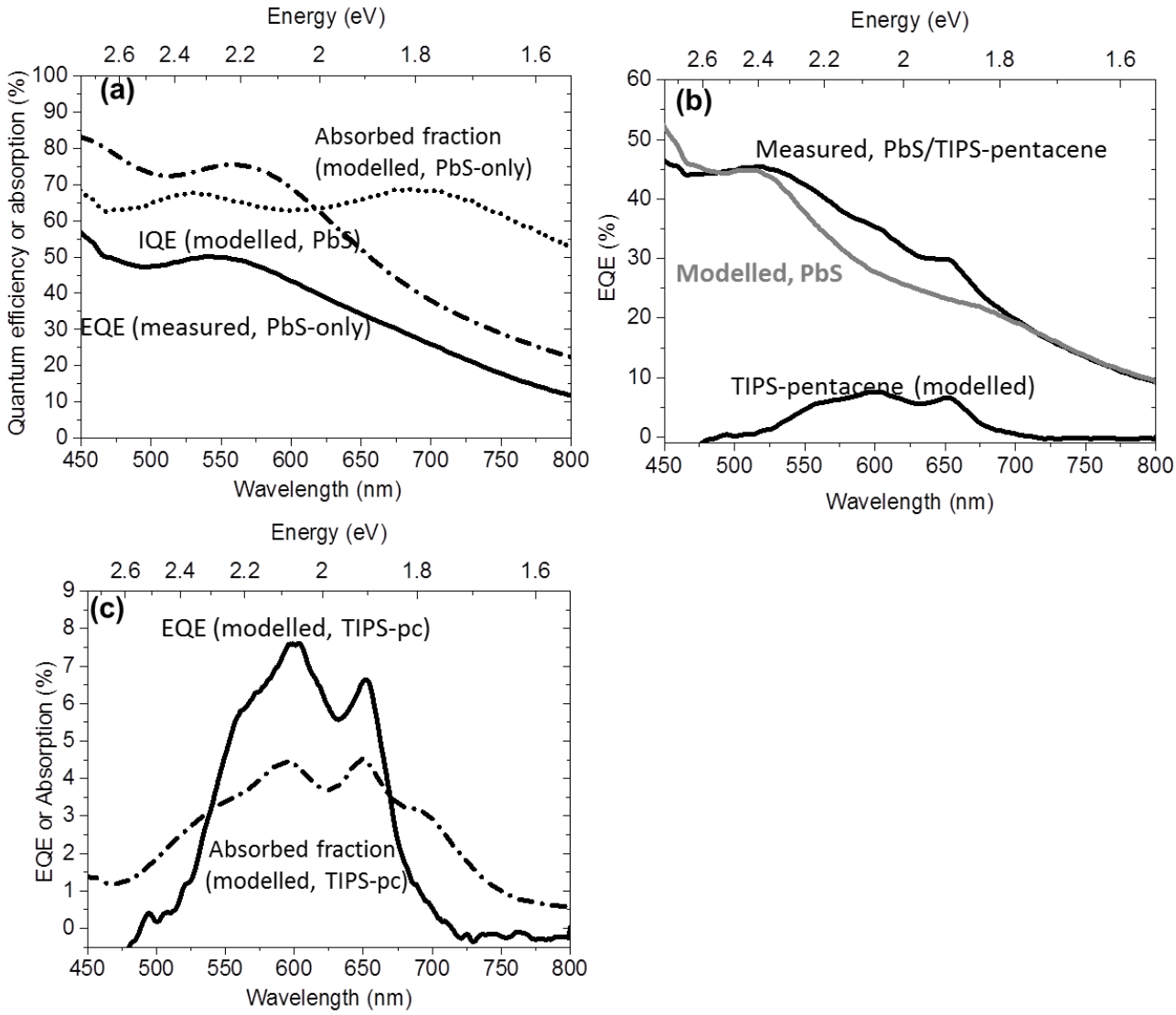

Figure S11 As above (**Figure S5**), for the 1.25 eV PbS and 1.25 eV PbS/TIPS-pentacene devices.

Table S4 Summary of layer thicknesses used in the transfer matrix optical modelling presented in **Figure S6-S8**.

	Thickness of Layers (nm)					
	ITO	**TiO_2**	**Nanocrystal**	**TIPS-pentacene**	**MoO_x**	**Au**
1.0 eV PbSe-only	125	30	100	--	12	80
1.0 eV PbSe / TIPS-pentacene	130	20	95	16	10	80
1.3 eV PbSe-only	130	30	90	--	12	80
1.3 PbSe / TIPS-pentacene	115	20	97	16	10	80
1.25 eV PbS-only	110	40	130	--	10	80
1.25 eV PbS / TIPS-pentacene	108	30	90	16	10	80

6.1 Range of Errors and Uncertainties on IQE calculations

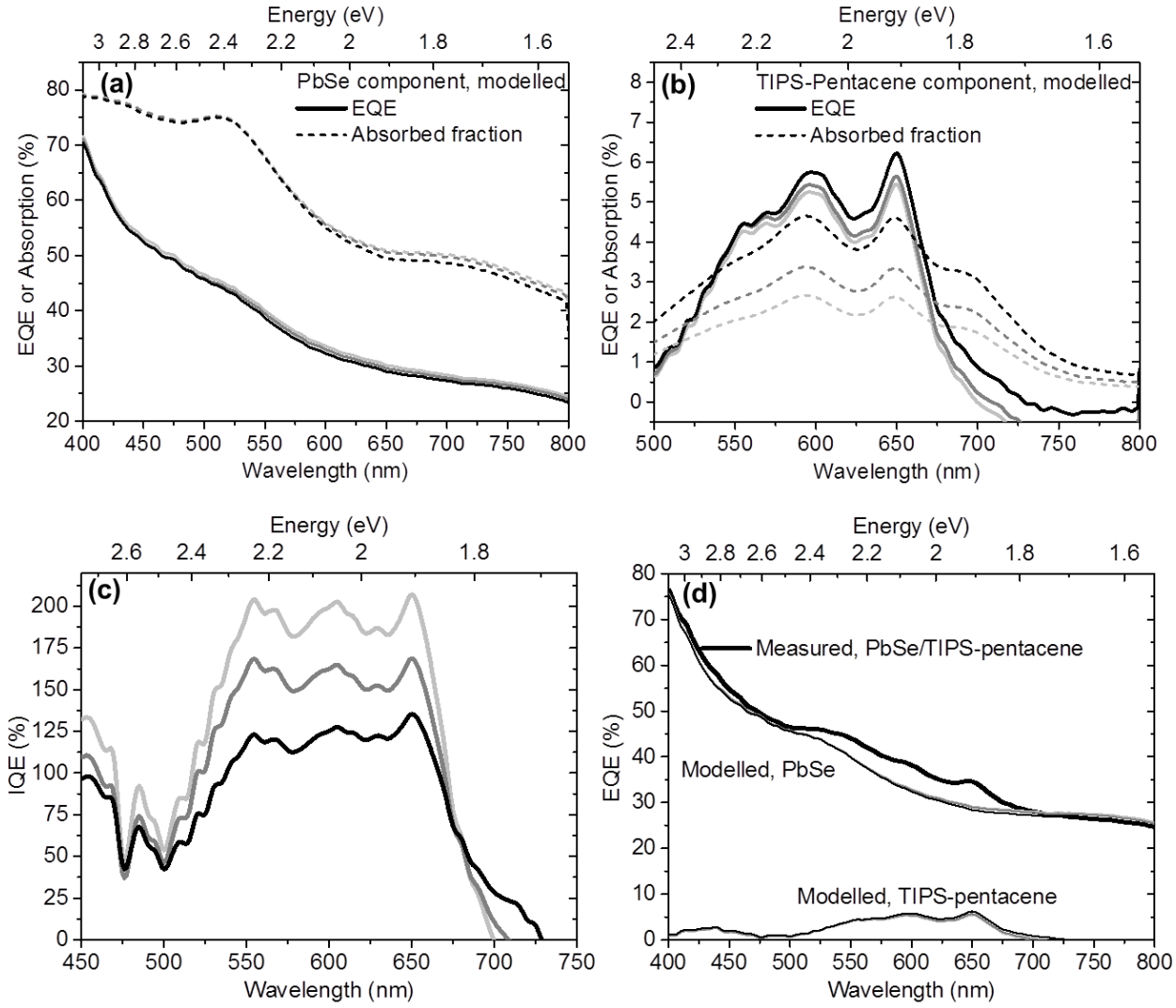

Figure S12 A range of parameters were fitted for the 1.0 eV PbSe/TIPS-pentacene system. In the optical model we used fixed values for TiO_2 (20 nm), PbSe (95 nm), MoO_x (10 nm), and Au (80 nm), and varied for ITO (128-133nm), and most significantly for TIPS-pentacene (13 nm, 16 nm and 20 nm). We used as wide a range of thicknesses for TIPS-pentacene as possible because of its inherent uncertainty in measuring such a thin film from AFM experimentally. This range of TIPS-pentacene thickness is consistent with those measured with XRD and ellipsometry. As the modelling is particularly sensitive to thin layers (i.e. TIPS-pentacene), we want to ensure that our IQE fitting is robust across the entire range of TIPS-pentacene thicknesses. We show here the results of those three sets of fits, with the two extreme cases (ITO 128 nm and TIPS-pentacene 20 nm in black; and ITO 133nm and TIPS pentacene 13 nm in light grey) and one average case (ITO 130nm and TIPS-pentacene 16 nm in grey). **(a)** Absorbed light fraction of the PbSe component (dash) and their contribution to the EQE (solid) by multiplying the light fraction with the IQE. **(b)** The corresponding EQE TIPS-pentacene component (solid), obtained by subtracting the solid curves in (a) from the measured device EQE (black thick solid, in (d)). Also shown here are the respective TIPS-pentacene absorbed light fractions (dash). **(c)** The range of corresponding TIPS-pentacene IQEs for the three sets of parameters, obtained by dividing the solid curves in (b) by their absorbed light fraction (dash, in (b)), indicating a value of 160±40%. **(d)** The curves in (a) and (b) compared to the measured EQE (black thick solid).

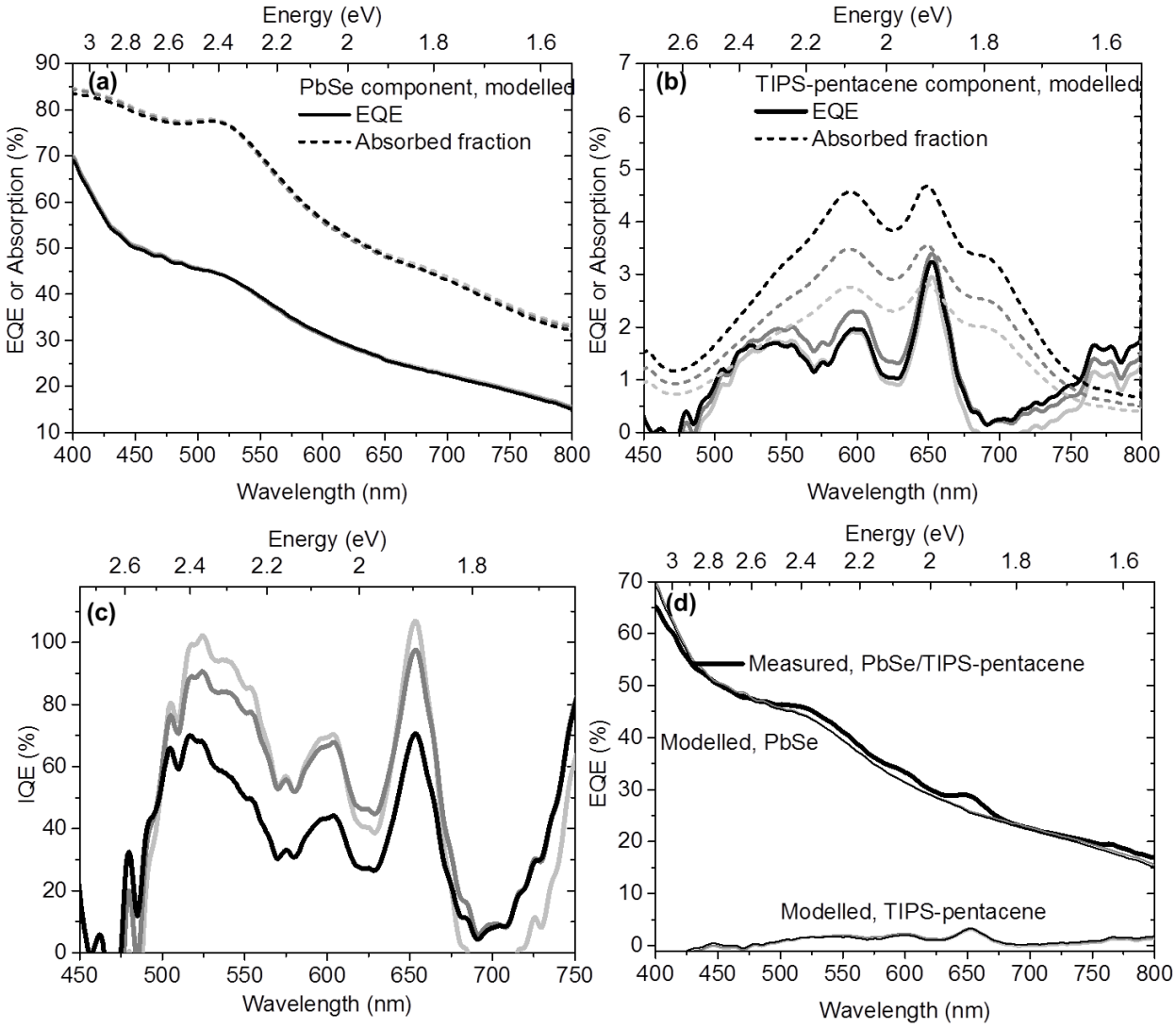

Figure S13 As above, for the 1.3 eV PbSe/TIPS-pentacene system. Similarly, values for TiO_2 (20 nm), MoO_x (10 nm), and Au (80 nm) were fixed, while ITO, PbSe and TIPS-pentacene were varied. ITO 115 nm, PbSe 97 nm, TIPS-pentacene 20 nm in black; ITO 120 nm, PbSe 97 nm, TIPS-pentacene 16 nm in grey; and ITO 120 nm, PbSe 98 nm, TIPS-pentacene 13 nm in light grey. We obtain an IQE of approximately 80±20%.

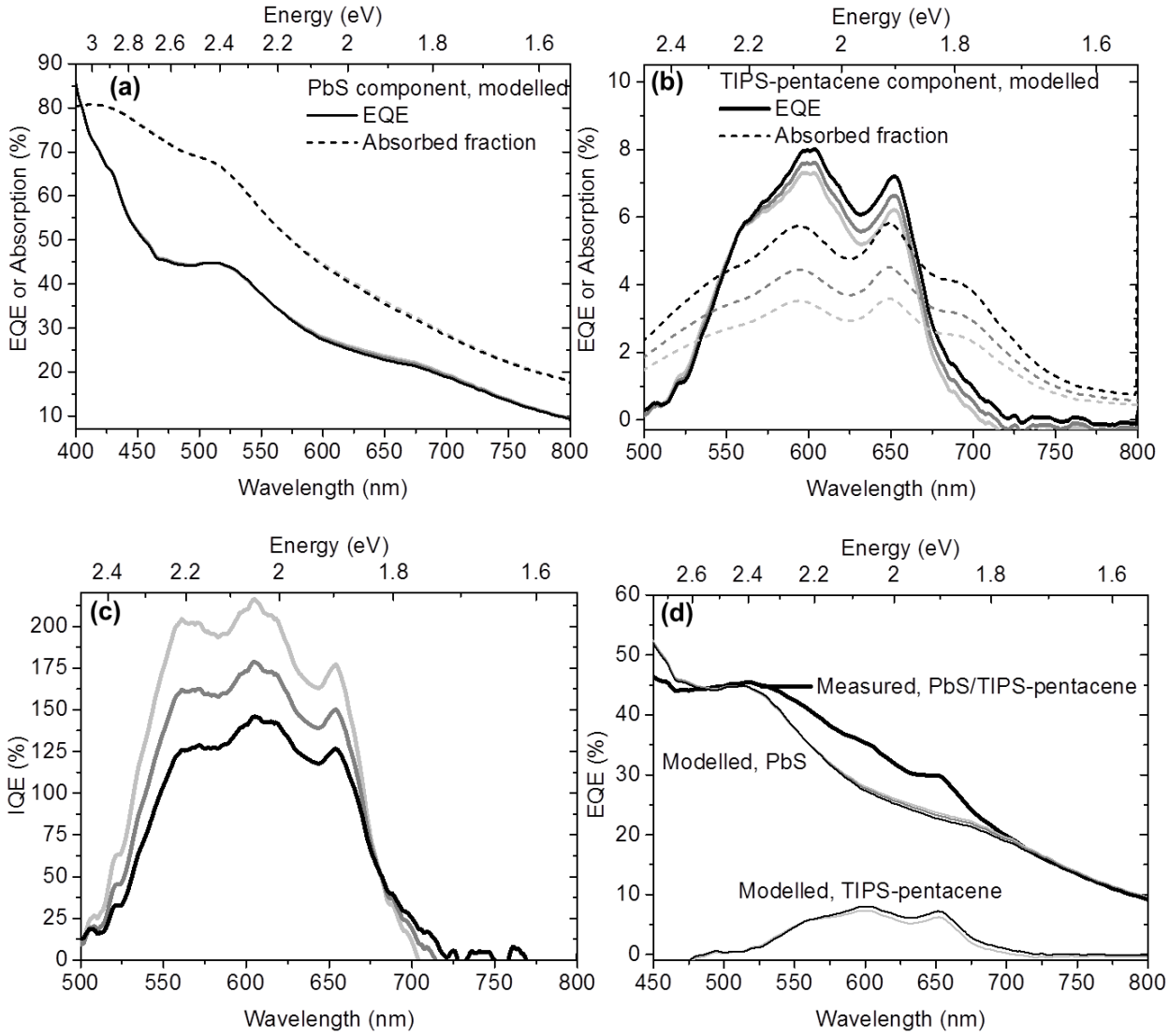

Figure S14 As above, for the 1.25 eV PbS/TIPS-pentacene system. Thicknesses of ITO (108 nm), TiO_2 (30 nm), PbSe (90 nm), MoO_x (10 nm) and Au (80 nm) were fixed, while that of TIPS-pentacene (20nm in black, 16 nm in grey, and 13 nm in light grey) was varied. An IQE of 170±30% is obtained.

REFERENCES

(1) Talapin, D. V; Lee, J.-S.; Kovalenko, M. V; Shevchenko, E. V. *Chem. Rev.* **2010**, *110*, 389–458.

(2) Luther, J. M.; Law, M.; Beard, M. C.; Song, Q.; Reese, M. O.; Ellingson, R. J.; Nozik, A. J. *Nano Lett.* **2008**, *8*, 3488–3492.

(3) Hines, M. A.; Scholes, G. D. *Adv. Mater.* **2003**, *15*, 1844–1849.

(4) Barkhouse, D. A. R.; Debnath, R.; Kramer, I. J.; Zhitomirsky, D.; Pattantyus-Abraham, A. G.; Levina, L.; Etgar, L.; Grätzel, M.; Sargent, E. H. *Adv. Mater.* **2011**, *23*, 3134–3138.

(5) Carnie, M. J.; Charbonneau, C.; Davies, M. L.; Troughton, J.; Watson, T. M.; Wojciechowski, K.; Snaith, H.; Worsley, D. a. *Chem. Commun. (Camb).* **2013**, *49*, 7893–7895.

(6) Luther, J. M.; Law, M.; Song, Q.; Perkins, C. L.; Beard, M. C.; Nozik, A. J. *ACS Nano* **2008**, *2*, 271–280.

(7) Heinemeyer, U.; Scholz, R.; Gisslén, L.; Alonso, M.; Ossó, J.; Garriga, M.; Hinderhofer, A.; Kytka, M.; Kowarik, S.; Gerlach, A.; Schreiber, F. *Phys. Rev. B* **2008**, *78*, 085210.

(8) Ehrler, B.; Walker, B. J.; Böhm, M. L.; Wilson, M. W. B.; Vaynzof, Y.; Friend, R. H.; Greenham, N. C. *Nat. Commun.* **2012**, *3*, 1019.

(9) Schubert, E. F. **2004**, Materials - Refractive index and extinction coefficient, retrieved from http://homepages.rpi.edu/~schubert/Educational-resources/Materials-Refractive-index-and-extinction-coefficient.pdf.

(10) Burkhard, G. F.; Hoke, E. T.; McGehee, M. D. *Adv. Mater.* **2010**, *22*, 3293–3297.

(11) Schubert, S.; Meiss, J.; Müller-Meskamp, L.; Leo, K. *Adv. Energy Mater.* **2013**, *3*, 438–443.